

# High-Fidelity Causal Video Diffusion Models for Real-Time Ultra-Low-Bitrate Semantic Communication

Cem Eteke<sup>✉</sup>, Batuhan Tosun<sup>✉</sup>, Alexander Griessel<sup>✉</sup>, Wolfgang Kellerer<sup>✉</sup>, *Fellow, IEEE*, and Eckehard Steinbach<sup>✉</sup>, *Fellow, IEEE*

**Abstract**—We introduce a video diffusion model for high-fidelity, causal, and real-time video generation under ultra-low-bitrate semantic communication constraints. Our approach utilizes lossy semantic video coding to transmit the semantic scene structure, complemented by a stream of highly compressed, low-resolution frames that provide sufficient texture information to preserve fidelity. Building on these inputs, we introduce a modular video diffusion model that contains Semantic Control, Restoration Adapter, and Temporal Adapter. We further introduce an efficient temporal distillation procedure that enables extension to real-time and causal synthesis, reducing trainable parameters by  $300\times$  and training time by  $2\times$ , while adhering to communication constraints. Evaluated across diverse datasets, the framework achieves strong perceptual quality, semantic fidelity, and temporal consistency at ultra-low bitrates ( $\leq 0.0003$  bpp), outperforming classical, neural, and generative baselines in extensive quantitative, qualitative, and subjective evaluations.

**Index Terms**—Real-time video synthesis, diffusion models, temporal distillation, semantic communication, ultra-low bitrate, video compression

## I. INTRODUCTION

GENERATIVE models have fundamentally changed how information can be processed. These models are increasingly capable of recovering high-quality data from sparse or degraded representations. This capability enables shifting the focus of communication applications from exact reconstruction toward generation under severe information constraints while preserving the quality of experience. A prominent line of work exploring such extended communication capabilities originates from semantic communication [1]. Early studies indeed demonstrated that transmitting implicit semantics, such as text or audio embeddings, results in robustness under noisy channel conditions while preserving the quality [2]–[5]. On top of the audio and text modalities, high-quality image and video generative capabilities of diffusion models naturally extended semantic communication to visual modalities: implicit semantic scene representations can condition generative models to generate perceptually high-quality content even when the

Cem Eteke, Batuhan Tosun, and Eckehard Steinbach are with the School of Computation, Information and Technology, Department of Computer Engineering, Munich Institute of Robotics and Machine Intelligence, Chair of Media Technology, Technical University of Munich, 80333 Munich, Germany. Corresponding author email: cem.eteke@tum.de

Alexander Griessel and Wolfgang Kellerer are with the School of Computation, Information and Technology, Department of Computer Engineering, Chair of Communication Networks, Technical University of Munich, 80333 Munich, Germany.

This work has been submitted to the IEEE for possible publication. Copyright may be transferred without notice, after which this version may no longer be accessible.

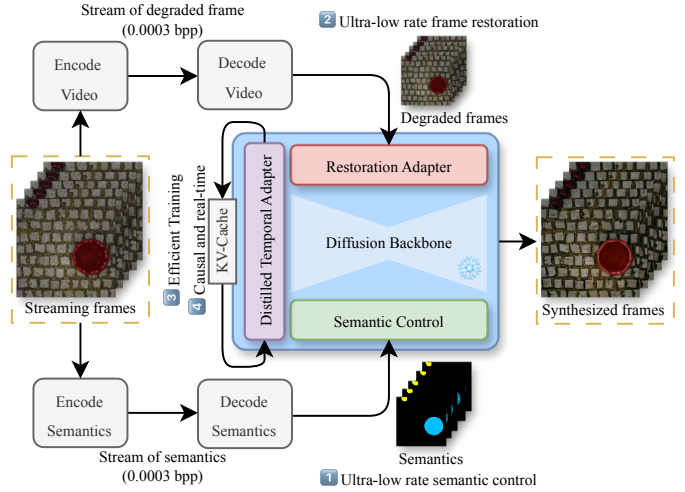


Fig. 1: Overview of our framework: ultra-low-bitrate scene semantics guide generation via Semantic Control, compressed low-resolution frames provide appearance cues through the Restoration Adapter, an efficiently distilled Temporal Adapter enables causal synthesis, and caching accelerates generation.

available input information is sparse or degraded [6]–[15]. However, reliance on implicit semantic information, mostly in the form of latent representations, effectively neglects the ultra-low-rate premise of semantic communication. [16]–[21].

For visual data, in contrast to implicit semantics (i.e., semantic latents), explicit semantics, such as facial landmarks or segmentation maps, enable ultra-low-bitrate image and video communication [22]–[29]. However, explicit semantics alone, which often lack sufficient appearance information, cannot maintain fidelity, especially across long sequences [30]–[32]. Moreover, semantic video communication requires communication-readiness, i.e., causal, temporally consistent, and real-time frame reconstruction or generation. Though controllable via explicit semantics at low bitrates, video diffusion models cannot satisfy these constraints due to their multi-step synthesis and bidirectional temporal modeling.

We address these challenges by introducing a novel semantic video synthesis model that maintains fidelity, perceptual quality, semantic fidelity, and temporal consistency within an ultra-low-bitrate semantic video communication framework. We utilize lossy contour-based IP-Frame semantic video compression and minimal texture cues in the form of low-resolution, highly compressed, degraded frames. Our model comprises Semantic Control for conditioning on ultra-low-rate semantics; Restoration Adapter for restoring ultra-low-

rate degraded frames; and Temporal Adapter for temporal consistency. We introduce efficient temporal distillation for causal, real-time, and autoregressive synthesis, achieving a fraction of the training cost:  $\times 300$  fewer parameters and  $\times 2$  shorter training time. We demonstrate that the modular structure further enables bitrate switching between control and restoration, and semantic adaptation. Finally, with the inclusion of key-value (KV) caching, we achieve performance towards real-time. Fig. 1 displays the overview.

Across two datasets with different scene characteristics, we show quantitatively that our method achieves high perceptual and semantic quality at bitrates as low as 0.0003 bpp, outperforming classical, neural, and generative baselines. In addition, we qualitatively demonstrate the efficacy and validate it through subjective evaluations.

To summarize, we introduce a novel communication-ready modular video diffusion model in a semantic video communication framework and present key contributions of:

- 1) Structured, ultra-low-bitrate semantic control through IP-Frame compressed videos of semantic maps to preserve scene structure.
- 2) Ultra-low-bitrate frame restoration that exploits highly compressed low-resolution frames to recover appearance cues and enhance fidelity.
- 3) Efficient distillation, converting a video diffusion model into a communication-ready few-step variant while significantly reducing training cost.
- 4) Real-time, autoregressive video synthesis enabled by causal temporal attention and key-value caching.

The remainder of the paper is organized as follows: Sec. II reviews related work, Sec. III introduces the relevant background, Sec. IV presents the novel video diffusion model and our semantic communication framework, Sec. V details the experimental setup, Section VI presents the results, and Section VII concludes the paper.

## II. RELATED WORK

We now review prior work in semantic communication, generative image and video compression, and diffusion-based restoration, which together form the basis of our approach.

### A. Semantic Communication

The feature extraction and generative capabilities of deep learning have made it central to semantic communication, where the goal is to transmit meaning [3], [33]. Most approaches treat latent representations as implicit semantics that constitute the meaning of a message [2]. For instance, text [3] and speech [4] semantic features have demonstrated robustness against channel noise. Generative models further enable the receiver to map decoded semantics to perceptual data under adverse conditions [14], relaxing the strict reconstruction constraint of classical communication and emphasizing perceptual quality over pixel fidelity [34]. This shift has motivated the integration of deep generative models into semantic communication [13], including the use of diffusion models (DMs) for audio inpainting [6] and denoising of latent semantics to improve robustness [15]. While latent semantics

offer strong resilience to channel impairments, operating at ultra-low bitrates remains challenging, particularly for visual communication, the most data-intensive modality.

To reduce bitrate demands, recent work has explored combining generative models with explicit semantics. Facial keypoints have enabled ultra-low-bitrate videoconferencing [35], but extending this paradigm to general scenes requires richer representations, such as semantic maps. Early methods combined latent and explicit semantics using GANs for semantic image communication [26], though latent semantics still incur higher rate requirements. More recent approaches utilize DMs to synthesize images from JPEG-compressed semantic maps, thereby improving robustness [12]. In parallel, contour-based lossy compression of semantic maps has been shown to better support ultra-low-bitrate synthesis [28]. While these advances improve resilience to channel noise, the literature places less emphasis on achieving ultra-low-bitrate operation. In contrast, our work specifically targets this regime.

### B. Generative Semantic Image Communication

Ultra-low bitrate generative semantic communication naturally intersects with deep image compression. Ballé et al. introduced learned transform coding for images [36], and later work relaxed the strict fidelity constraint through perceptual and generative criteria [34], emphasizing realism over pixel accuracy. Agustsson et al. applied generative models to image compression [11]. With the superior synthesis capability of diffusion models [37], [38], latent DMs have been adopted for generative latent coding via transform coding in latent space [9]. However, these methods still depend on semantic latents, which impose high bitrates.

To address this, recent work leverages explicit semantics and controllable DMs to enable lower rates. Pretrained DMs provide strong priors and effective control mechanisms [39], motivating hybrid strategies that combine latent and explicit semantics [18]. Scene-level control signals have been explored through semantic maps [25], semantic filtering of scene graphs to reduce transmitted information [30], and transform-coded semantic latents used as DM control inputs [17]. Other works combine multimodal explicit semantics, such as text and sketches, to guide compression [23]. Semantic maps, in particular, have proven highly bit-efficient [27]. Pezone et al. combined explicit semantics with low-resolution frames for low-bitrate generative semantic communication with DMs [40]. These approaches compress the explicit semantics losslessly. Recent studies show that generative models can tolerate distortions introduced by lossy semantic map compression, enabling ultra-low bitrate semantic image communication [28].

### C. Generative Semantic Video Communication

The principles of ultra-low-bitrate generative semantic image communication naturally extend to video, albeit with stricter temporal and computational constraints. Classical codecs such as HEVC [41] and VVC [42], as well as neural video codecs such as DCVC [43], exploit motion information on P-Frames in combination with image compression on I-Frames. In the generative domain, Li et al. employed DMs

to extrapolate future frames from traditionally compressed I-Frames [16]. Related approaches synthesize I-Frames from semantic latents while relying on traditional codecs for P-Frames [20]. The performance of these hybrid methods is constrained by the codecs. Recurrent GANs have been used to generate temporally consistent frames from compressed latent semantics [19], and generative latent coding has been extended to videos via temporally buffered latent semantics [7], later enhanced using DM-based synthesis [8]. As with images, however, semantic latents often impose bitrate overhead compared to explicit semantics.

To reduce the rate, researchers extended lossy semantic coding to an I-Frame/P-Frame structure for semantic maps, enabling ultra-low bitrate semantic video compression [31]. However, when video frames are synthesized solely from explicit semantics using video DMs, significant fidelity degradation occurs over time. To mitigate this, Wan et al. combined controllable DMs for explicit semantic synthesis with deep image compression for latent-based I-Frames [44]. Image-to-Video (I2V) synthesis has also been integrated into lossy semantic video coding to preserve scene information through a guiding frame [32]. Although these hybrid methods improve fidelity, their reconstruction quality remains strongly dependent on the bitrate of the transmitted frames, and degradations accumulate. Furthermore, temporal modeling in these approaches is typically bidirectional, which prevents them from supporting the autoregressive, real-time synthesis required in a communication scenario. These limitations highlight the need for an explicit restoration mechanism to recover perceptual fidelity when information is heavily compressed, as well as for causal temporal modeling for real-time generation.

#### D. Restoring and Real-Time Generative Semantic Video Communication

Pezone et al. utilized downsampled frames for low-rate guidance [40]. Although downsampling reduces the rate, DMs can restore complex degradations. Recent work has explored applying large multimodal models for semantic or prompt-guided image compression [22], [29], where compact descriptors or extremely compressed image cues guide generative restoration. While effective for images, these approaches remain slow, operate at the image level only, and lack mechanisms for causal temporal synthesis. Few-step diffusion models have also been proposed for generative video compression [21], but they rely on latent semantics and do not leverage explicit semantics that enable ultra-low bitrate. Restoration-oriented diffusion models, such as the distillation-based method of Zhou et al. for superresolving compressed videos [45], improve fidelity but require large models, target higher bitrates, and do not incorporate explicit semantics. Moreover, their extension to causal, autoregressive video synthesis is unclear, which limits their suitability for semantic communication.

To overcome these limitations, we propose a modular, controllable, and restoring video diffusion model that integrates ultra-low-bitrate neural video codecs and ultra-low-bitrate explicit semantics. Our model is composed of three

key components: (i) Semantic Control, which enables semantic fidelity, (ii) Restoration Adapter, which enhances perceptual fidelity, and (iii) Temporal Adapter, which enforces temporal consistency and enables autoregressive and causal video synthesis. Our method enables adaptation to various semantics and bitrates. We further introduce an efficient distillation scheme, specifically applied to the Temporal Adapter, which substantially reduces training costs while maintaining synthesis quality.

### III. BACKGROUND

In this section, we introduce the preliminaries for our approach: the key concepts of latent diffusion models, attention mechanisms, and distillation.

#### A. Latent Diffusion Models

Diffusion models are trained for inverting a forward diffusion process. The forward process starts from a noise-free vector  $x_0$  and introduces noise to it at each diffusion timestep  $t$ , defining a forward diffusion process as

$$q(x_t | x_{t-1}) = \mathcal{N}(x_t; \sqrt{\alpha_t}x_{t-1}, (1 - \alpha_t)I).$$

Using this forward model, the direct mapping between any  $x_t$  given  $x_0$  could be computed as

$$q(x_t | x_0) = \mathcal{N}(x_t; \sqrt{\bar{\alpha}_t}x_0, (1 - \bar{\alpha}_t)I) \quad (1)$$

where  $\bar{\alpha}_t$  is the scheduling parameter's accumulated version  $\bar{\alpha}_t = \prod_{i=0}^{t-1} \alpha_i$ . A diffusion model  $\epsilon_\theta$  learns to invert Eq. 1 as

$$p_\theta(x_{t-1} | x_t) = \mathcal{N}(\mu_\theta(x_t, t), \Sigma_\theta(x_t, t)), \quad (2)$$

where the parameters  $\mu_\theta$  and  $\Sigma_\theta$  are parameterized by the diffusion model  $\epsilon_\theta$  given  $x_t$  and  $t$ . The diffusion denoising probabilistic modeling (DDPM) trains the model to minimize

$$\mathcal{L}_D = \mathbb{E} \left[ \left\| \varepsilon - \epsilon_\theta(\sqrt{\bar{\alpha}_t}x_0 + \sqrt{1 - \bar{\alpha}_t}\epsilon, t) \right\|_2^2 \right] \quad (3)$$

where  $\varepsilon := x_T \sim \mathcal{N}(0, I)$ , the noise that generates the observation  $x_t$  as given in Eq. 2.

Though DDPM has been shown to significantly outperform GANs, training proved unstable and required substantial computational resources [37]. Latent Diffusion Models (LDMs) resolved this issue by performing synthesis in the latent space [38]. The input to  $\epsilon_\theta$  is hence extracted from an image  $I$  using an encoder  $\mathcal{E}$ , such that  $x_0 = \mathcal{E}(I)$ .

After optimizing for Eq. 1,  $\epsilon_\theta$  samples clean latents, i.e.,  $x_0$ , by solving the parameterized inverse diffusion process iteratively, starting from  $x_T \sim \mathcal{N}(0, I)$ . To introduce stability to this inverse process, Denoising Diffusion Implicit Models (DDIM) estimate clean latents, namely  $x_{t \rightarrow 0}$ , for guidance and utilize the update rule of

$$x_{t-1} = \sqrt{\bar{\alpha}_{t-1}}x_{t \rightarrow 0} + \sqrt{1 - \bar{\alpha}_{t-1}}\epsilon_\theta(x_t, t),$$

where the estimated noise-free latents are the solution to the forward model in Eq. 1

$$x_{t \rightarrow 0} = \left( \frac{x_t - \sqrt{1 - \bar{\alpha}_t}\epsilon_\theta(x_t, t)}{\sqrt{\bar{\alpha}_t}} \right). \quad (4)$$

### B. Attention Mechanism

Introduced in the Transformer architecture, attention enables dynamic weighting of features based on their relevance to themselves, namely self-attention, or to other modalities, namely cross-attention [46]. These relevance scores are the similarity between the query vector  $Q$  and the key vector  $K$ . Let  ${}^n z_t$  be the output of  $n^{\text{th}}$  hidden layer of  $\epsilon_\theta$ . Self-attention is then computed as

$$\text{attention}(Q, K, V) = \text{softmax}\left(\frac{QK^T}{\sqrt{d_n}}\right)V$$

where  $Q = {}^n z_t W^Q$ ,  $K = {}^n z_t W^K$ , and  $V = {}^n z_t W^V$ . The parameter set  $\{W^Q, W^K, W^V\}$  forms the trainable attention weights.

### C. Latent Consistency Models

Latent Consistency Models (LCMs) accelerate diffusion sampling by distilling a full teacher diffusion model into a student that can skip multiple denoising steps at once [47]. Instead of executing all reverse diffusion steps, LCMs simulate a jump from a later timestep,  $t+s$ , directly to an earlier timestep  $t$  using an ODE solver:  $\Psi(x_{t+s}, t+s, t)$ .

A student model with parameters  $\theta^-$  is then trained to match the teacher's predictions on these skipped trajectories. Given the simulated latent  $\hat{x}_t = x_{t+s} + \Psi(x_{t+s}, t+s, t)$ , the student is supervised via

$$\mathcal{L}_{\text{LCM}} = \mathbb{E}\left[\|\epsilon_{\theta^-}(\hat{x}_t, t) - \epsilon_\theta(x_t, t)\|_2^2\right]. \quad (5)$$

By learning consistency across skipped steps, the student can reproduce the teacher's behavior with only a few evaluations during inference, enabling efficient few-step diffusion.

### D. Distribution Matching Distillation

Diffusion Matching Distillation (DMD) aims to achieve, like LCM, synthesis from a few steps by training the student model to skip steps while ensuring that the resulting samples remain aligned with the teacher [48]. Given a noise-free estimate  $\hat{x} := \hat{x}_{t \rightarrow 0}$  from  $\epsilon_{\theta^-}(\hat{x}_t, t)$  via Eq. 4, DMD minimizes the divergence between the real and generated distributions of  $\hat{x}$  through a KL-Divergence objective

$$\mathcal{L}_{\text{DMD}}(p_{\text{fake}} \| p_{\text{real}}) = \mathbb{E}[-\log p_{\text{real}}(\hat{x}) - \log p_{\text{fake}}(\hat{x})]$$

which has the following gradient

$$\nabla_{\theta^-} \mathcal{L}_{\text{DMD}} = \mathbb{E}\left[-(s_{\text{real}}(\hat{x}) - s_{\text{fake}}(\hat{x})) \frac{d\hat{x}}{d\theta^-}\right]. \quad (6)$$

where score functions  $s_{\text{real}}$  and  $s_{\text{fake}}$  are the log-gradients of the probability densities. Diffusion models estimate this score as noise-free latents  $\hat{x}_{t \rightarrow 0}$  for a step  $t \in \mathcal{U}[t_{\min}, t_{\max}]$  sampled during training. In this context,  $s_{\text{real}}$  is estimated through the teacher network while  $s_{\text{fake}}$  utilizes a third network  $\epsilon_{\theta^{\text{fake}}}$ , namely the critic. Both use the formulation in Eq. 4, but with their respective parameters.

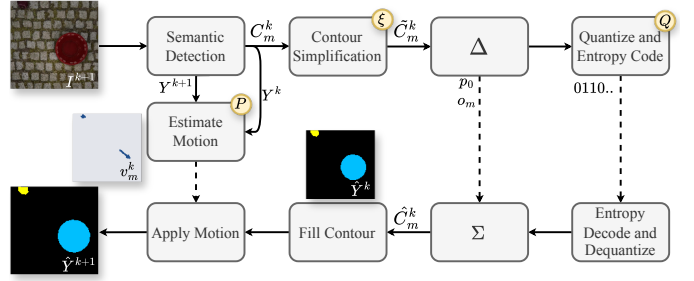


Fig. 2: Semantic video coding pipeline. Contours extracted from semantic object masks are simplified with a tolerance  $\xi$ , then differentially encoded, quantized to  $Q$  symbols, and entropy-coded. For P-frames, selected via the I-frame period  $P$ , only semantic motion is transmitted.

In this formulation the teacher  $\epsilon_\theta$  is frozen but the student model  $\epsilon_{\theta^-}$  and the critic  $\epsilon_{\theta^{\text{fake}}}$  are trained. This training is done in an oscillating manner. First, the student is optimized through  $\mathcal{L}_{\text{DMD}}$  in Eq. 6 then the critic is optimized through  $\mathcal{L}_{\text{D}}$  in Eq. 3. The student learns synthesis in a few steps, while the critic updates the distribution to fit the student. By matching score functions rather than relying solely on regression, DMD improves distillation stability and enables high-fidelity few-step generation.

## IV. METHODOLOGY

In Fig. 1, we present the overall pipeline of our novel, communication-ready, generative semantic video communication approach. Our approach has two main components: (i) semantic video compression and (ii) semantic video synthesis. The former enables ultra-low bitrate, while the latter enables real-time high-quality video communication. In this section, we dive into the details of these two main parts.

### A. Semantic Video Coding

For an I-frame at video timestep  $k$ , i.e., when  $k \bmod P = 0$ , the semantic map  $Y^k$  is decomposed into disjoint instance contours by identifying class boundaries and separating non-connected regions. We represent each semantic instance  $m$  in the local pixel neighborhood  $\mathcal{N}$  of  $Y^k$  as an ordered set of 2D contour points:

$$M^k = \{(i, j) \mid Y^k(i, j) = m \wedge \exists (i', j') \in \mathcal{N} : Y^k(i', j') \neq m\}.$$

The set  $M^k$  is then split into disjoint connected components  $C_m^k$  such that

$$M^k = \bigcup_m C_m^k.$$

Finally, every instance is represented as a set of coordinates, i.e.,  $C_m^k := \{p_{m0}, p_{m1}, \dots \mid p_{mi} \in \mathbb{R}^2\}$ , by tracing the boundary points in a clockwise order.

We used line simplification with tolerance  $\xi$  to create the reduced set of contours  $\tilde{C}_m^k$  that represent the same shape with fewer contour points. The simplified contour is then

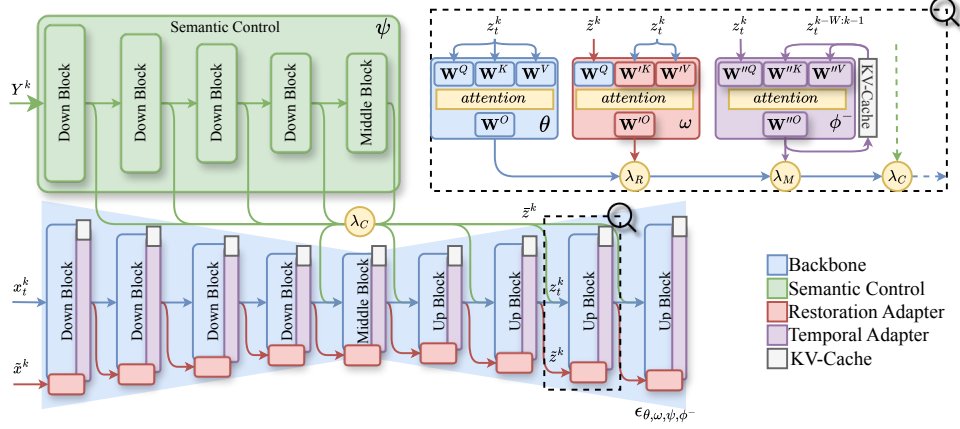


Fig. 3: The overall architecture of our video diffusion model that extends a frozen backbone. The model takes as input the diffused latents  $x_t^k$ , degraded latents  $\tilde{x}^k$ , and semantics  $Y^k$  of frame  $k$ . Semantic Control injects features extracted from  $Y^k$  into the backbone. The Restoration Adapter uses degraded features  $\tilde{z}^k$  as queries in a restoration attention module. Temporal Adapter applies temporal attention between the current features  $z_t^k$  and cached features  $z_t^{k-W:k-1}$  causally.

differentially encoded. The first point of each instance  $p_{m0}$  and the instance identifier, i.e., the class label,  $o_m$ , are transmitted explicitly, and all remaining points are represented as increments

$$\Delta \tilde{C}_m^k = \{p_{m1} - p_{m0}, p_{m2} - p_{m1} \dots\}.$$

The differentials  $\Delta \tilde{C}_m^k$  are quantized uniformly using  $Q$  symbols and entropy coded via arithmetic coding, yielding a compact representation of the entire contour. At the receiver, inverse quantization and cumulative summation reconstruct the contour  $\hat{C}_m^k$ , which is finally rasterized into a dense semantic map to reconstruct the semantics as

$$\hat{Y}_m^k(i, j) = o_m \mathbb{1}[(i, j) \in \mathcal{R}(\hat{C}_m^k)].$$

For P-frames, we reuse the previously decoded semantic map  $\hat{Y}^k$  and transmit only instance-wise motion  $v_m$  and label  $o_m$ . We estimate a rigid translation vector  $v_m^k \in \mathbb{R}^2$  for each instance  $m$  as the shift in the centroid

$$v_m^k = \left[ \mu_m^{k+1} - \mu_m^k \right], \quad \mu_m^k = \frac{\sum_{i,j} (i, j) \mathbb{1}[Y^k(i, j) = o_m]}{\sum_{i,j} \mathbb{1}[Y^k(i, j) = o_m]}.$$

At the receiver, contour instances in  $\hat{Y}^k$  are shifted to yield the next semantic map  $\hat{Y}^{k+1}$  such that

$$\hat{Y}_m^{k+1}(i, j) = \hat{Y}_m^k(i - v_m^k(1), j - v_m^k(2)),$$

This approach enables us to represent videos of semantic maps at ultra-low bitrates. Fig. 2 illustrates the steps described in the semantic video coding methodology.

### B. Semantic Video Synthesis

The goal of the semantic video synthesis module is to map ultra-low-bitrate semantics to a high-fidelity, temporally consistent video stream in real time. To achieve this, we introduce a novel modular video diffusion model that consists of; (i) Semantic Control that injects explicit semantics, (ii) Restoration Adapter that exploits highly compressed frames, and (iii) distilled Temporal Adapter that models temporal interactions and

enables causal, autoregressive synthesis, rendering the method communication-ready. The modularity not only enables plug-and-play operation across different operating points but also enables low-complexity adaptation to different semantics and efficient distillation of the Temporal Adapter. Fig. 3 displays the overall architecture.

1) *Diffusion Backbone*: We start from a pretrained LDM  $\epsilon_\theta$ , trained to minimize the standard diffusion loss  $\mathcal{L}_D$  in Eq. (3). We provided further details in Sec. III-A. Here we extend the previous formulation to include the video timestep  $k$ . Given an input frame  $I^k$ , the encoder  $\mathcal{E}$  produces a latent  $x_0^k = \mathcal{E}(I^k)$ , on which the forward diffusion process is utilized as in Eq. (1). At denoising timestep  $t$ , the backbone predicts the noise  $\epsilon_\theta(x_t^k, t)$  and is used to iteratively construct  $x_{t-1}^k$ .

Architecturally,  $\epsilon_\theta$  is composed of multiple downsampling, bottleneck, and upsampling blocks, each of which contains self-attention layers, the mechanism of which is described in Sec. III-B. We denoted the output of layer  $n$  at diffusion step  $t$  for frame  $k$  as  ${}^n z_t^k$  in Sec. III-B. For clarity, we omit the layer index  $n$  in the remainder of this section. In our framework, all backbone parameters  $\theta$  remain frozen; all semantic communication functionality is introduced exclusively through lightweight adapters that modulate these intermediate features.

2) *Semantic Control*: If we iteratively solve the inverse diffusion process starting from  $x_T^k \sim \mathcal{N}(0, I)$  without any conditioning, the model synthesizes random frames unrelated to the transmitted content. To turn the backbone into a semantic video communication system, we extend it with control parameters  $\psi$  to a conditional model

$$\epsilon_{\theta, \psi}(x_t^k, Y^k, t),$$

where  $Y^k$  represents the explicit semantics of frame  $k$ . In our case,  $Y^k$  is the ultra-low-bitrate semantic map produced by the contour-based semantic video codec, as described in Sec. IV-A. Here, we dropped the notation  $\hat{Y}$  for simplicity.

Either directly retraining LDMs or training from scratch with semantic conditioning is impractical due to the scale of data and computation required, especially when conditioning

is applied to densely reconstructed semantic maps. However, large-scale LDMs have been shown to be controllable through fine-tuning small adapter architectures or by adding semantic features to residual connections [39]. Taking advantage of the strength of our modular approach, we utilize these semantic residuals to enable synthesis from dense reconstruction of ultra-low-bitrate semantic maps. This approach utilizes a clone of the encoder, namely  $\epsilon_\psi$ . The output of each cloned layer  $\bar{z}^k$  is injected at the decoder

$$z_t^k \leftarrow z_t^k + \lambda_C \bar{z}^k,$$

where  $z_t^k$  denotes the activations of the backbone, and  $\lambda_C \in [0, 1]$  controls the strength of Semantic Control.

This mechanism enables the backbone to respect the scene structure conveyed by  $Y^k$  while still freely synthesizing fine details. Since the semantics are transmitted via the contour-based codec, their bitrate cost is extremely small. This is further enabled by generative models, which are robust to moderate semantic distortions, thereby largely mitigating semantic compression-induced errors during the synthesis process [28].

3) *Restoration Adapter*: While explicit semantics efficiently capture what is present in the scene, they do not preserve all appearance details. To improve fidelity at ultra-low bitrates, we additionally transmit low-resolution, heavily compressed frames, i.e., degraded frames  $\tilde{I}^k$ . Their bitrate footprint is still small, but they provide useful cues about texture, color, and illumination. To take advantage of this information, we extend the backbone with restoration parameters  $\omega$  to incorporate the information from the degraded frames

$$\epsilon_{\theta, \psi, \omega}(x_t^k, \tilde{x}_t^k, Y^k, t),$$

where  $\tilde{x}^k = \mathcal{E}(\tilde{I}^k)$  is the latent of the degraded frame.

At each layer, the backbone produces degraded features  $\tilde{z}^k$  parallel to  $z_t^k$ . LDMs preserve the similarity between clean and degraded frames; hence, the attention mechanism can be extended by a few parameters for frame restoration, again leveraging the modular structure [49]. The Restoration Adapter extends the self-attention to also attend to these features using them as the query

$$\begin{aligned} z_t^k &\leftarrow \text{attention}(Q, K, V) W^O \\ &+ \lambda_R \text{attention}(\tilde{Q}, K', V') W'^O, \end{aligned} \quad (7)$$

where  $\tilde{Q} = \tilde{z}^k W^Q$ ,  $K' = z_t^k W'^K$ , and  $V' = z_t^k W'^V$ . The scalar  $\lambda_R \in [0, 1]$  controls the strength of the restoration. Importantly, we keep  $W^Q$  fixed and only train the small set of parameters  $\{W'^K, W'^V, W'^O\}$  on top of the frozen backbone, which constitutes the set  $\omega$ . Control parameters  $\psi$  are omitted during the training of  $\omega$ .

Intuitively, the degraded features query the latent space for their clean counterparts, allowing the model to restore high-frequency details guided by the compressed frames. Because the adapter is lightweight and the backbone remains frozen, this Restoration Adapter can be switched on or off based on available bitrate and application constraints, without retraining the main model.

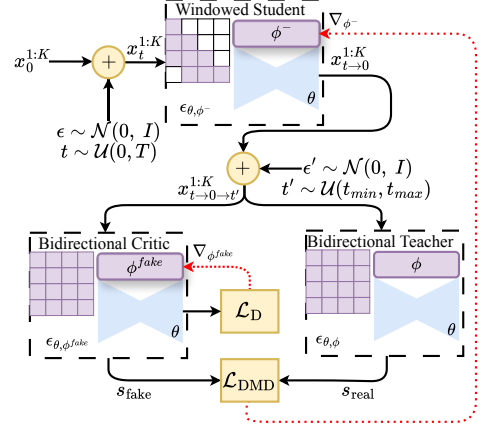


Fig. 4: Efficient distillation of the Temporal Adapter  $\phi^-$ . Red-dotted lines denote the gradients.

4) *Temporal Adapter*: While Semantic Control and Restoration Adapter enable the model to synthesize high-fidelity frames conditioned on ultra-low-bitrate semantic information, both operate independently on each frame. This is sufficient for still-image generation but leads to unacceptable temporal inconsistencies in real-time semantic video communication. To ensure temporal consistency, we further extend the model with a Temporal Adapter  $\phi$  that explicitly models the temporal relationships between frames.

Let  $z_t^{1:K} \in \mathbb{R}^{K \times D \times (H \times W)}$  denote the stacked spatial features of  $K$  consecutive frames at diffusion step  $t$ . To apply attention along the temporal dimension, we reshape this tensor to  $z_t^{1:K} \in \mathbb{R}^{(H \times W) \times D \times K}$ . The Temporal Adapter augments the backbone self-attention with temporal attention,

$$\begin{aligned} z_t^{1:K} &\leftarrow \text{attention}(Q, K, V) W^O \\ &+ \lambda_T \text{attention}(Q'', K'', V'') W''^O, \end{aligned} \quad (8)$$

where  $Q'', K'', V''$  are computed from  $z_t^{1:K}$  using the temporal-attention weights  $\{W''^Q, W''^K, W''^V, W''^O\}$  and  $\lambda_T \in [0, 1]$  controls the contribution of temporal modeling. The collection of all temporal-attention parameters constitutes the set  $\phi$ . We apply the Temporal Adapter after the Restoration Adapter, as temporality should be accounted for in the final versions of the frames. The overall model becomes

$$\epsilon_{\theta, \omega, \psi, \phi}(x_t^{1:K}, \tilde{x}_t^{1:K}, Y^{1:K}, t).$$

Through this mechanism, the Temporal Adapter learns how motion and appearance evolve across frames, enabling the model to propagate consistent structure, dynamics, and visual attributes over time while keeping the backbone parameters  $\theta$  frozen and preserving the modular nature. As we will discuss in the next section, our method further enables efficient distillation to meet the requirements of communication readiness.

5) *Autoregressive and Real-Time Synthesis*: Diffusion models require many steps for high-quality synthesis. Furthermore, the Temporal Adapter described above operates on a fixed set of  $K$  frames with bidirectional temporal attention. This method is suitable for offline video generation, but it is not aligned with the requirements of semantic video communication, where frames must be synthesized in a causal, autoregres-

sive, and real-time manner, where jointly processing  $K$  frames would imply large memory consumption, high computational cost per update, and an intrinsic delay proportional to  $K$ .

To overcome these issues, we extend the Temporal Adapter into a causal, windowed variant via a distillation procedure. Enabled by the modular nature, we keep the rest frozen for efficient training. Concretely, we regard the model  $\epsilon_{\theta, \phi}(x_t^{1:K}, t)$  with unconstrained temporal attention as a teacher. We then train a student Temporal Adapter with parameters  $\phi^-$ , i.e.,  $\epsilon_{\theta, \phi^-}(x_t^{k-W:k}, t)$ , where  $\phi^-$  is initialized from  $\phi$ . Different from  $\epsilon_{\theta, \phi}$ , the student,  $\epsilon_{\theta, \phi^-}$ , only attends to a small causal window of size  $W$ ; at the same time, it learns to reproduce the teacher's output in fewer diffusion steps by skipping intermediate steps. For this purpose, we optimized the DMD loss presented in Eq. 6. We used the teacher to estimate the real score  $s_{\text{real}}$  and a critic  $\epsilon_{\theta, \phi^{\text{fake}}}(x_t^{1:K}, t)$  to estimate the fake score  $s_{\text{fake}}$ . The critic parameters  $\phi^{\text{fake}}$  are also initialized from the teacher,  $\phi$ , and it uses bidirectional temporal attention. As described in Sec. III-D it models the student's output distribution. We would like to point out that, unlike the conventional approaches, we only distill the adapter weights. This allows parameter-efficient training.

We achieve causal training by applying masking to the temporal attention of  $\epsilon_{\theta, \phi^-}(x_t^{1:K}, t)$ . Let  $i$  and  $j$  denote temporal indices  $1 : K$ , and we define the temporal attention mask as

$$M_{ij} = \begin{cases} 1, & \text{if } \left\lfloor \frac{j-1}{W} \right\rfloor \leq \left\lfloor \frac{i-1}{W} \right\rfloor, \\ 0, & \text{otherwise.} \end{cases} \quad (9)$$

This mask enforces that each frame can only attend to itself and a fixed number of past frames, but never to the future. This distillation approach is presented in Fig. 4. In this way, the student inherits the temporal priors of the full model while operating under causality to support autoregressive synthesis, resulting in a reduced temporal context and fewer diffusion steps, thereby improving efficiency.

Finally, combining the modules discussed above, we present our novel video diffusion model for ultra-low-bitrate semantic communication

$$\epsilon_{\theta, \omega, \psi, \phi^-}(x_t^{k-W:k}, \tilde{x}_t^{k-W:k}, Y^{k-W:k}, t).$$

Even with windowed attention, naively recomputing the temporal attention's keys and values for all frames in the window would incur unnecessary overhead in streaming scenarios. To further improve efficiency, we employ key-value (KV) caching in the Temporal Adapter: once the keys and values of a past frame have been computed, they are stored and reused for subsequent frames as long as they remain within the active window [50]. For an arriving frame  $k$ , only the corresponding query, key, and value of the frame need to be computed, and the temporal attention reuses the cached keys and values of the previous frames  $k - W : k - 1$ .

The combination of (i) a distilled, causal, windowed Temporal Adapter and (ii) KV caching yields an autoregressive synthesis process with constant per-frame complexity and a delay of at most  $W - 1$  frames. Together with the Semantic



Fig. 5: Example videos from the YCB-Sim dataset.

Control and Restoration Adapters, this enables our video diffusion model to operate in a communication-ready regime: it produces temporally consistent video frames autoregressively as semantic information becomes available, operates in real-time, and facilitates ultra-low-bitrate transmission at high perceptual quality and semantic fidelity. Fig. 3 displays the overall architecture.

## V. SETUP & EXPERIMENTS

To demonstrate the effectiveness of our approach, we conduct a series of experiments evaluating both semantic video coding and synthesis. In this section, we outline the experimental setup and key implementation details.

### A. Datasets

We evaluate our method on two datasets that differ in scene structure, motion complexity, and semantic density. This enables us to evaluate the robustness and generalizability of our approach.

1) *Cityscapes*: Cityscapes is a widely used benchmark for urban scene understanding [51]. It provides 5,000 training videos and 500 validation videos. Each video depicts complex street scenes and features a single frame of a finely annotated semantic map. We use a resolution of  $256 \times 512$  pixels and a frame rate of 10 frames per second.

2) *YCB-Sim*: To evaluate performance on object-interaction scenarios, we generated a simulated dataset using Blender-Proc [52] and the publicly available YCB object set [53]. For each video, we randomly sample table textures, lighting conditions, and object subsets. Objects are dropped and subjected to random forces to induce rich interactions and non-rigid motions. We render videos at a resolution of  $512 \times 512$  and 10 frames per second, and collected 10,000 videos with semantic labels from a top-down camera. We present example frames from the dataset in Fig. 5.

### B. Ultra-Low-BitRate Semantic Video Coding

Our semantic video codec, described in Sec. IV-A, is governed by three parameters that control the rate and semantic distortion: the contour simplification tolerance  $\xi$ , the I-Frame period  $P$ , and the number of quantization symbols  $Q$ . We begin by analyzing the effect of each parameter on the semantic fidelity, measured by the mean intersection over union (mIoU),

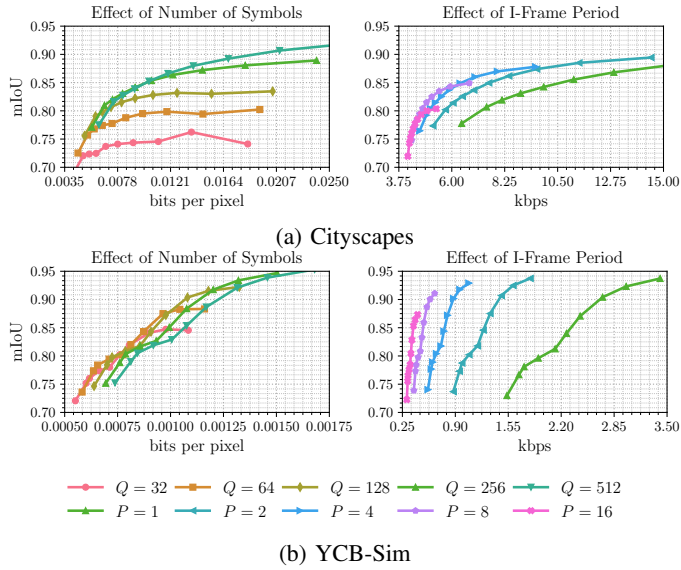


Fig. 6: The semantic rate-distortion curves. We investigate the effect of the number of quantization symbols  $Q$  and the I-Frame period  $P$ , where we control the bitrate on the x-axis by setting the contour simplification tolerance  $\xi \in [4, 24]$ .

across both datasets. The results are summarized in Fig. 6. Throughout the experiments, we sweep  $\xi \in [4, 24]$ , which serves as the primary rate-control parameter for each choice of  $P$  and  $Q$ , allowing us to study their interactions.

1) *Effect of  $Q$  and  $\xi$ :* Parameters  $Q$  and  $\xi$  jointly determine the bitrate of I-Frames. The resulting rate-distortion curves, shown in Fig. 6, indicate that  $Q = 256$  consistently offers the best trade-off between compression efficiency and semantic fidelity. In both datasets, the configuration  $Q = 256$  and  $\xi = 6$  achieves  $\text{mIoU} \geq 0.85$  while enabling ultra-low-bitrate operation: approximately 0.011 bpp on Cityscapes and 0.001 bpp on YCB-Sim.

2) *Effect of  $P$  and  $\xi$ :*  $P$  determines the number of P-frames following each I-frame. Fixing  $Q = 256$  and sweeping  $\xi$  as before, we obtain the curves presented in Fig. 6. The analysis reveals that  $P = 4$  provides the most favorable balance between rate reduction and semantic distortion. Larger values of  $P$  introduce increased distortion, while smaller values reduce coding efficiency by transmitting I-Frames too frequently.

3) *Final Configuration:* Based on these findings, we use  $Q = 256$ ,  $P = 4$ , and  $\xi = 6$  for all remaining experiments. Under this configuration, we operate at two bitrates: 7 kbps ( $\frac{7 \times 1024}{256 \times 512 \times 10} = 0.0054$  bpp) on Cityscapes and 1 kbps ( $\frac{1 \times 1024}{512 \times 512 \times 10} = 0.0003$  bpp) on YCB-Sim. These values reflect the intrinsic structural differences between the datasets. Cityscapes contains dense, large-scale urban scenes with complex object boundaries, naturally requiring more bits to encode. In contrast, YCB-Sim features comparatively sparse tabletop arrangements with fewer, well-separated semantic instances, allowing the contour-based representation to reach substantially lower bitrates. Evaluating these two qualitatively different datasets enables a comprehensive assessment of our method.

### C. Ultra-Low-Bitrate Video Coding

An essential component of our framework is the use of low-resolution, highly compressed, i.e., degraded frames to provide appearance cues that semantic synthesis alone cannot recover. For example, relying solely on semantic maps may lead to ambiguities, such as a car being synthesized facing the wrong way. To provide minimal yet informative visual guidance, we simply allocate the same bitrate to these degraded frames across all datasets. We employ the DCVC neural video codec [43] at 4× lower spatial resolution, operating at 7 kbps for Cityscapes and 1 kbps for YCB-Sim. When combined with our ultra-low-bitrate semantic maps, the total budget becomes 14 kbps (0.0108 bpp) for Cityscapes and 2 kbps (0.0006 bpp) for YCB-Sim. This setup provides a compact yet effective appearance signal that complements the Semantic Control and significantly improves fidelity.

### D. Semantic Video Synthesis Implementation and Training

In this section, we describe the architectural components used to realize the novel video diffusion model presented in Sec. IV-B, along with the corresponding training procedures and key hyperparameters. All modules are trained using 4× NVIDIA RTX Pro 6000 Blackwell GPUs with the AdamW optimizer and a weight decay of  $10^{-2}$  [54].

1) *Diffusion Backbone:* As described in Sec. IV-B1, our approach relies on a pretrained and frozen latent diffusion backbone. We use Stable Diffusion [55] as the underlying denoiser, operating with an empty text prompt since no textual conditioning is required. This backbone provides a strong image prior for high-quality synthesis, and keeping it fixed stabilizes training across all modules while allowing each adapter to specialize efficiently.

2) *Semantic Control:* To steer the synthesis toward the transmitted semantic maps, we use an injection-based control mechanism as described in Sec. IV-B2. For this purpose, we employ ControlNet [39] and train separate sets of control parameters  $\psi$  for Cityscapes and YCB-Sim. Our modular approach allows us to switch between datasets without retraining the full model. We train the control module on labeled frames from each dataset using a batch size of 16 (effective batch size  $16 \times 4 = 64$ ), a learning rate of  $2 \times 10^{-6}$ , and gradient clipping of 1 for  $10^5$  iterations. The objective is the diffusion loss in Eq. 3, computed using the backbone extended with the Semantic Control,  $\epsilon_{\theta, \psi}(x_t, Y_t, t)$ . This module plays a crucial role in preserving scene structure and ensuring that synthesized frames retain semantic fidelity.

3) *Restoration Adapter:* To incorporate the low-resolution, compressed frames into the synthesis process, we employ the BIR-Adapter described in Sec. IV-B3 [49]. This module learns restoration-specific attention parameters  $\omega$  that guide the diffusion backbone toward the clean latent features corresponding to the degraded inputs. We train the adapter using a combination of DIV2K [56], DIV8K [57], and Flickr2K [58], applying a widely used degradation model that includes 4× downsampling, noise, blur, and compression artifacts [59]. Training uses random  $512 \times 512$  patches, a batch size of 16 (effective  $16 \times 4 = 64$ ), a learning rate of  $10^{-5}$ , and  $10^5$

iterations while minimizing the diffusion loss in Eq. 3 evaluated with the restoration-extended backbone  $\epsilon_{\theta, \omega}(x_t, \tilde{x}_t, t)$ . This adapter proves essential for recovering appearance cues that semantics alone cannot provide.

*4) Temporal Adapter and Distillation:* To equip the frozen diffusion backbone with temporal consistency, we introduce a temporal attention mechanism as described in Sec. IV-B4, implemented using a pretrained AnimateDiff model with video length  $K = 16$  [60]. We extend this model to support communication-ready, autoregressive synthesis as detailed in Sec. IV-B5, which requires converting the bidirectional temporal attention into a causal, windowed variant and reducing the number of diffusion steps. DMD was shown to be effective in this context [61]. We apply DMD, however, to distill only the Temporal Adapter parameters  $\phi$  of the model  $\epsilon_{\theta, \phi}$  while keeping the diffusion backbone fixed. Our approach allows the temporal component to be trained in isolation, substantially reducing training cost compared to full-model distillation. The student is initialized using Latent Consistency Models (LCM) with a window size of  $W = 3$ , sampling  $10^3$  videos from the teacher, followed by  $8 \times 10^3$  LCM update steps, given in Eq. 5. After this initialization, DMD is performed for  $50 \times 10^3$  on the OpenVid-1M dataset [62], using a batch size of 6 (effective  $6 \times 4 = 24$ ). The student is trained to minimize the KL term in Eq. 6, and the critic is trained to minimize the diffusion loss in Eq. 3. As shown in Fig. 4, the student employs causal while the critic uses bidirectional attention.

After training the three modules, namely the Semantic Control, Restoration Adapter, and Temporal Adapter, separately, we combine them in to the model  $\epsilon_{\theta, \omega, \psi, \phi^-}(x_t^{k-3:k}, \tilde{x}_t^{k-3:k}, Y^{k-3:k}, t)$  and extend it with KV-caching to enable efficient and high-quality autoregressive synthesis. When run on an NVIDIA RTX 4090 at a resolution of  $512 \times 512$  with  $T = 4$  diffusion steps and a window size of  $W = 3$ , our approach achieves towards real-time generation, without any special optimizations, at ultra-low bitrates, producing 5.1 FPS while using 6.2 GB of VRAM.

## E. Metrics

We evaluate our approach using a combination of reference-based and reference-free metrics. For frame-level fidelity, we report PSNR and MS-SSIM. For perceptual quality, we utilize LPIPS [63] and DISTS. To assess semantic consistency, we compute the mean Intersection over Union (mIoU) between the outputs of a semantic segmentation model applied to the synthesized and ground-truth frames. In addition, we employ VBench [64] for reference-free video evaluation and report the metrics most relevant to our setting: Imaging Quality, Aesthetic Quality, and Motion Smoothness, which do not rely on text conditioning. Together, these metrics capture fidelity, perceptual quality, semantic fidelity, and temporal consistency, enabling us to clearly identify the aspects in which our method offers consistent improvements.

## F. Baselines

We compare our approach with a range of conventional, neural, and generative video compression methods. We used,

as conventional codecs, HEVC<sup>1</sup> [65] and VVC<sup>2</sup> [66] with default parameters. As a neural codec, we evaluate DCVC [43]. For generative ultra-low bitrate compression, we use Extreme Video Coding (EVC) [16]. In addition, we compare our approach with I2V-SC [32], an image-to-video semantic communication framework that uses the same diffusion backbone and temporal module of a fixed number of frames  $K = 16$ . To test for causal generation performance on  $K = 30$ , we use the distilled Temporal Adapter in I2V-SC. Together, these baselines encompass classical, neural, and generative paradigms, enabling a comprehensive comparison.

## G. Ablation Studies

We also conduct several ablation studies to examine the influence of each module and parameter on the overall performance.

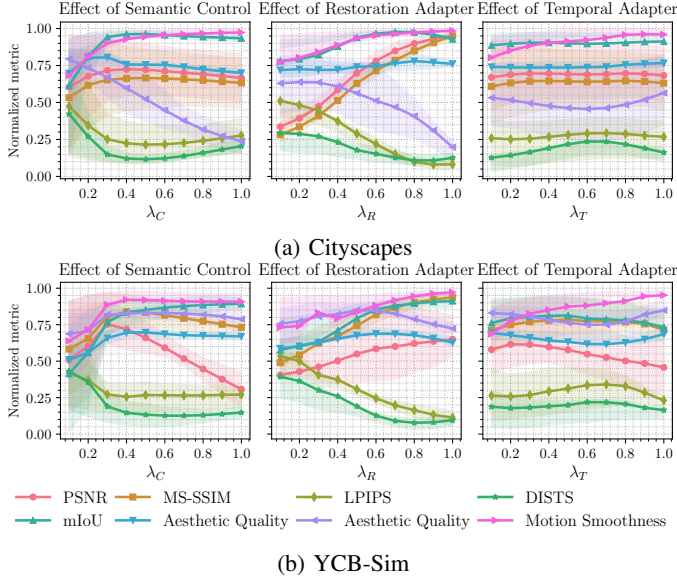
*1) Module Weights:* We first examine the three weighting parameters that control the relative contribution of each module:  $\lambda_C$  for Semantic Control,  $\lambda_R$  for the Restoration Adapter, and  $\lambda_T$  for the Temporal Adapter, as described in Sec. IV and illustrated in Fig. 3. For both datasets, we selected 25 videos and performed a grid search over these three parameters, sweeping each within  $[0, 1]$  in increments of 0.1, resulting in a total of 25,000 evaluated configurations. This analysis demonstrates how each module contributes to successful synthesis and how its interactions influence overall performance. Fig. 7 presents the effect of each weight.

*2) Efficient Distillation:* As discussed in Sec. IV-B5, we distill only the Temporal Adapter parameters  $\phi$ , rather than the full model  $\epsilon_{\theta, \phi}$ , which substantially reduces the number of trainable parameters and enables an efficient distillation process. To evaluate this novel approach, we compare the temporal-adapter-only distilled model  $\epsilon_{\theta, \phi^-}$  with both the non-distilled teacher  $\epsilon_{\theta, \phi}$  and a fully distilled variant  $\epsilon_{\theta^-, \phi^-}$ . Since this analysis focuses purely on the temporal behavior, we treat it as a text-to-video synthesis task and employ the full VBench evaluation suite. This experiment highlights how isolating the temporal module enables efficient training while preserving the performance of the teacher model. Fig. 8 compares the performance, and Tab. I reports the required training resources.

*3) Effect of Restoration and Control:* As described earlier, the overall bitrate is divided between two information sources: (i) the semantic maps, handled by the Semantic Control module, and (ii) the low-resolution neural video codes, processed by the Restoration Adapter. To analyze their individual contributions, we disable each adapter at two operating points. This allows us to evaluate performance both when only half of the bitrate is used, because one module is inactive, and when the full bitrate is allocated to a single active module. These experiments demonstrate how the two components complement each other and how the modular structure enables flexible rate allocation, while maintaining improved performance compared to existing approaches. In Table II, we also include the results obtained by disabling the aforementioned modules.

<sup>1</sup><https://trac.ffmpeg.org/wiki/Encode/H.265>

<sup>2</sup><https://github.com/fraunhoferhhi/vvenc>

Fig. 7: Effect of module weights  $\lambda_C$ ,  $\lambda_R$ , and  $\lambda_T$ .

#### H. Subjective Evaluation

Reference-based metrics, particularly pixel-level measures such as PSNR and MS-SSIM, do not fully capture the perceptual behavior of generative models, especially under the perception–distortion trade-off [34]. Reference-free metrics, while useful, can also be influenced by the underlying video models. For this reason, we additionally conducted a subjective evaluation. Participants were presented with two reconstructed versions of the same video and were asked to indicate a binary preference based on overall visual quality. One option corresponded to our approach, while the other corresponded to a baseline, with randomized positions. For each dataset, we selected 6 random test videos from 5 baselines, resulting in  $2 \times 6 \times 5 = 60$  comparisons per participant. We conducted the study with 12 participants, following ethics committee approval and informed consent. No personal data is recorded.

## VI. RESULTS & DISCUSSION

### A. Effect of Module Weights

We begin by analyzing the influence of the three weighting parameters introduced in Sec. IV, namely the Semantic Control weight  $\lambda_C$ , the Restoration Adapter weight  $\lambda_R$ , and the Temporal Adapter weight  $\lambda_T$ . As discussed in Sec. V-G1, for both datasets, we evaluate the average normalized metric values obtained by fixing one parameter and sweeping the others between  $[0, 1]$ . We present the results in Fig. 7.  $\lambda_C$  consistently improves semantic preservation and perceptual quality up to approximately 0.4, after which improvements begin to saturate.  $\lambda_T$  shows minimal effect on PSNR and MS-SSIM, but strongly improves perceptual quality and motion smoothness when  $\lambda_T = 1.0$ , demonstrating its importance for temporally coherent autoregressive synthesis.  $\lambda_R$  improves both fidelity, as measured by PSNR and MS-SSIM, and perceptual quality, as assessed by LPIPS and DIST, although values above 0.8 negatively impact performance. Based on

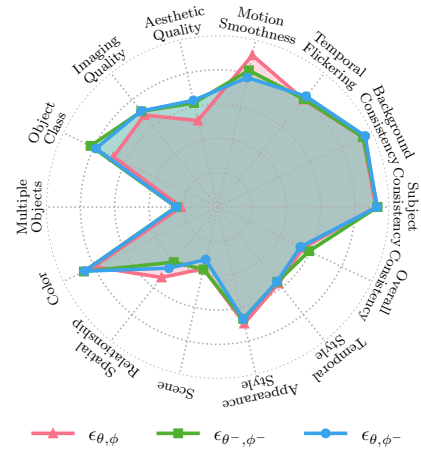


Fig. 8: Radar plot of the V-Bench text-to-video evaluation comparing the teacher model  $\epsilon_{\theta, \phi}$ , the distillation of backbone and Temporal Adapter  $\epsilon_{\theta^-, \phi^-}$ , and our Temporal Adapter-only distillation  $\epsilon_{\theta, \phi^-}$ . All perform comparably.

TABLE I: Comparison of full and temporal distillation. Our approach requires significantly fewer training resources. 300 $\times$  reduction in parameters and 2 $\times$  reduction in GPU hours.

Method	Parameters	Batch	Accumulation	GPU Hours
$\epsilon_{\theta^-, \phi^-}$	$1.3 \times 10^9$	2	3	12.5
$\epsilon_{\theta, \phi^-}$	$4.1 \times 10^6$	6	1	6

these observations, we use  $\lambda_C = 0.4$ ,  $\lambda_T = 1.0$ , and  $\lambda_R = 0.8$  for all the experiments. These findings highlight the complementary roles of the three modules of our novel method outlined in Sec. IV.

### B. Efficient Temporal Adapter Distillation

As discussed in Sec. IV-B5, we distill only the Temporal Adapter parameters  $\phi$ , while keeping the diffusion backbone fixed. This reduces training cost significantly. To evaluate this choice, we compare the teacher model  $\epsilon_{\theta, \phi}$ , a fully distilled model  $\epsilon_{\theta^-, \phi^-}$ , and our temporal-only distilled model  $\epsilon_{\theta, \phi^-}$ . The radar plot in Fig. 8 shows that all three models achieve similar performance across motion, appearance, and consistency metrics. However, as summarized in Table I, our temporal-only distillation requires substantially fewer training resources, while providing almost twice the training speed compared to a fully distilled model. The teacher model performs similarly but cannot be later used in a communication setting that requires causal, real-time video synthesis. This large-scale evaluation already establishes the effectiveness and efficiency of selectively distilling the temporal module. Therefore, in our semantic communication framework, we focus on assessing performance under causal constraints.

### C. Quantitative Results

We compare the full model  $\epsilon_{\theta, \omega, \phi, \psi^-}$  with the baselines introduced in Sec. V-F and with the ablated variants that disable Semantic Control ( $\lambda_C = 0$ ) or restoration ( $\lambda_R = 0$ ),

TABLE II: Quantitative comparison on Cityscapes and YCB-Sim at different bit rates. For LPIPS and DISTs lower is better ( $\downarrow$ ). We highlight for each bit rate the **best**, **second-best**, and **top-3** performances.

(a) Cityscapes									
Bit rate (kbps / bpp)	Method	PSNR	MS-SSIM	LPIPS $\downarrow$	DISTS $\downarrow$	mIoU	Aesthetic Quality	Imaging Quality	Motion Smoothness
7 / 0.0054	HEVC	23.41	0.81	0.57	0.33	0.36	0.34	0.26	0.98
	VVC	<b>23.98</b>	<b>0.84</b>	0.55	0.33	0.42	0.34	0.27	<b>0.99</b>
	DCVC	<b>25.83</b>	<b>0.88</b>	0.43	0.29	0.61	0.41	0.33	0.99
	EVC	18.05	0.62	0.49	0.31	0.64	0.42	0.31	<b>0.99</b>
	I2V-SC	15.88	0.5	<b>0.39</b>	<b>0.21</b>	<b>0.87</b>	<b>0.5</b>	<b>0.66</b>	0.96
	$\lambda_R = 0$	14.37	0.49	0.5	0.3	<b>0.81</b>	<b>0.47</b>	0.41	0.98
	$\lambda_C = 0$	21.89	0.83	<b>0.37</b>	<b>0.23</b>	0.77	0.43	<b>0.51</b>	0.98
14 / 0.0108	HEVC	24.45	0.86	0.53	0.31	0.39	0.36	0.27	0.98
	VVC	<b>25.0</b>	<b>0.89</b>	0.5	0.3	0.52	0.37	0.29	<b>0.99</b>
	DCVC	<b>27.24</b>	<b>0.92</b>	0.35	0.26	0.7	0.44	0.35	0.99
	EVC	17.95	0.62	0.47	0.3	0.69	0.41	0.32	<b>0.99</b>
	I2V-SC	15.84	0.5	0.39	<b>0.21</b>	<b>0.86</b>	<b>0.5</b>	<b>0.66</b>	0.96
	$\lambda_R = 0$	13.51	0.42	0.49	0.27	0.84	<b>0.47</b>	0.57	0.97
	$\lambda_C = 0$	17.26	0.82	<b>0.34</b>	0.22	0.82	0.43	0.55	0.97
(b) YCB-Sim									
Bit rate (kbps / bpp)	Method	PSNR	MS-SSIM	LPIPS $\downarrow$	DISTS $\downarrow$	mIoU	Aesthetic Quality	Imaging Quality	Motion Smoothness
1 / 0.0003	HEVC	<b>25.06</b>	<b>0.74</b>	<b>0.58</b>	<b>0.34</b>	0.31	0.33	0.27	<b>0.99</b>
	VVC	22.98	0.55	0.76	0.53	0.08	0.2	0.18	0.99
	DCVC	<b>27.14</b>	<b>0.71</b>	0.6	0.39	0.56	0.31	0.3	<b>0.99</b>
	EVC	16.51	0.5	0.77	0.52	0.08	0.27	0.19	0.99
	I2V-SC	19.58	0.44	<b>0.47</b>	<b>0.29</b>	<b>0.82</b>	<b>0.4</b>	<b>0.67</b>	0.96
	$\lambda_R = 0$	16.68	0.36	0.64	0.34	<b>0.74</b>	<b>0.42</b>	<b>0.68</b>	0.97
	$\lambda_C = 0$	19.79	0.64	0.67	0.36	0.49	0.34	0.56	0.97
2 / 0.0006	HEVC	<b>25.81</b>	<b>0.75</b>	0.57	0.33	0.32	0.33	0.27	<b>0.99</b>
	VVC	24.13	0.61	0.72	0.46	0.18	0.23	0.2	0.99
	DCVC	<b>27.71</b>	<b>0.75</b>	0.57	0.37	0.63	0.32	0.32	<b>0.99</b>
	EVC	16.9	0.55	0.73	0.46	0.15	0.3	0.23	0.99
	I2V-SC	19.54	0.43	<b>0.47</b>	<b>0.29</b>	<b>0.79</b>	<b>0.4</b>	<b>0.67</b>	0.96
	$\lambda_R = 0$	16.58	0.35	0.64	0.34	0.69	<b>0.41</b>	<b>0.68</b>	0.97
	$\lambda_C = 0$	19.7	0.66	0.63	0.34	0.53	0.35	0.59	0.97

as discussed in Sec. V-G3. We evaluate all methods using the metrics defined in Sec. V-E. As described in Sec. V-C, we allocate equal bitrates to the low-resolution degraded frames and the semantic video codes. When either signal is disabled for ablation, the total bitrate is halved. For completeness, we also report the performance of the ablated models when the bitrate is doubled, matching the operating point of the full system. The results are summarized in Table II.

Conventional codecs (HEVC [65], VVC [66]) and neural video codec (DCVC [43]) achieve higher PSNR and MS-SSIM values. However, they perform poorly on perceptual metrics (LPIPS, DISTs), semantic consistency (mIoU), and reference-free video quality measures (Aesthetic and Imaging Quality). This confirms that pixel fidelity metrics alone are insufficient in the presence of generative synthesis and the perception-distortion trade-off. The generative semantic video communication baseline I2V-SC [32], which utilizes the same Temporal Adapter but relies on a guidance frame for image-to-video synthesis, performs worse than ours on semantic and perceptual metrics, underscoring the benefits of our method.

The ablation study highlights the contribution of each module. Disabling the Restoration Adapter ( $\lambda_R = 0$ ) results in a significant decrease in PSNR and perceptual quality, highlighting its role in recovering appearance cues from highly compressed frames. Disabling Semantic Control ( $\lambda_C = 0$ ) results in a substantial drop in mIoU, confirming that explicit semantic guidance is essential for preserving scene structure while enabling quick adaptation to different semantic types, thanks to modularity. Despite these degradations, both ablated variants remain competitive and surpass most baselines, illustrating the robustness of our modular framework. Furthermore, since disabling either module halves the operating bitrate, the results indicate that our approach maintains strong perceptual performance even at extremely low bitrates of 0.0054 bpp (Cityscapes) and 0.0003 bpp (YCB-Sim). It is worth noting that HEVC outperformed VVC in the extremely low-bitrate regime on the YCB-Sim dataset. The underlying reason for this behavior is beyond the scope of this work.



Fig. 9: Qualitative results at bitrates 0.094, 0.0064, and 0.0007 bpp from top to bottom.

#### D. Qualitative Results

To support our quantitative results and their discussion, we present qualitative results in Fig. 9. This figure displays example videos from both datasets, generated using our approach and the baselines. These results demonstrate how our

method achieves higher quality compared to classical and neural codecs, and how it preserves fidelity better, for example, in the case of non-rigid motion of a rotating cup, compared to the semantic communication baseline I2V-SC. Fig. 10 presents qualitative results illustrating the effects of the ablation study.

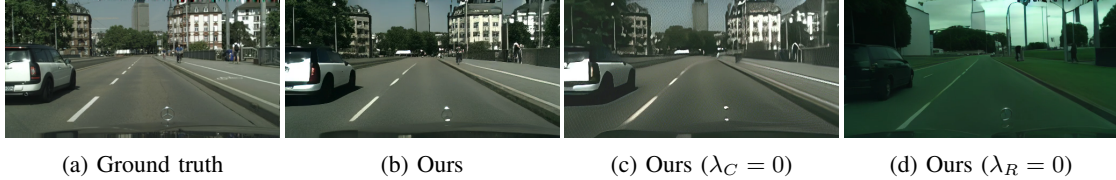


Fig. 10: Visual results of the ablation study. Removing Semantic Control ( $\lambda_C = 0$ ) leads to degraded semantic consistency, while removing the Restoration Adapter ( $\lambda_R = 0$ ) reduces perceptual fidelity.

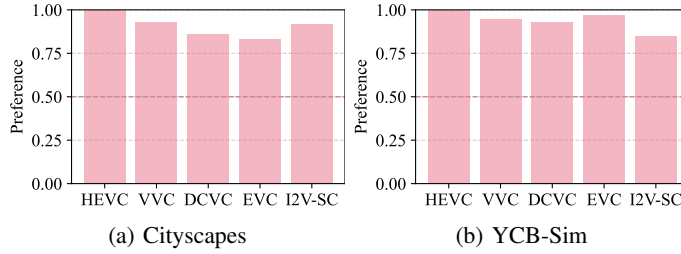


Fig. 11: Subjective preference of our method.

### E. Subjective Evaluation

Objective metrics do not fully capture perception, particularly in generative settings. Therefore, we conducted a subjective evaluation as described in Sec. V-H. Participants viewed pairs of reconstructed videos and reported their preference. Across both datasets, our approach was consistently preferred over all baselines. We present the average subjective preference compared to the baselines in Fig. 11. As pointed out in Sec. VI-C, HEVC unexpectedly outperformed VVC on YCB-Sim. However, subjective evaluations suggest otherwise.

These results highlight the advantages of our modular diffusion-based generative semantic video communication framework. It achieves superior semantic preservation, perceptual quality, and temporal consistency, both quantitatively and qualitatively, and is constantly preferred by participants, while being communication-ready with real-time causal and autoregressive synthesis.

## VII. CONCLUSION

This work presented a modular video diffusion model with Semantic Control, Restoration Adapter, and Temporal Adapter within an ultra-low-bitrate generative semantic video communication framework. By integrating semantic video compression with highly compressed low-resolution frames, our approach operates under extreme bitrate constraints while preserving fidelity. The modular design not only enables flexible bitrate allocation but also supports an efficient distillation strategy that yields a communication-ready, i.e., causal and real-time temporal model, with significantly reduced training complexity:  $300\times$  fewer trained parameters and  $2\times$  less training time. Extensive quantitative, qualitative, and subjective evaluations demonstrate consistent improvements in semantic fidelity and visual quality at bitrates as low as 0.0003 bpp.

Nevertheless, the current implementation is limited in the frame rate, which constrains high-frame-rate deployment. In addition, while the adopted diffusion backbone delivers strong,

stable performance, more recent large-scale generative architectures may further enhance synthesis quality and scalability. Importantly, such architectural advances are complementary to our diffusion model modules and communication framework and do not alter their underlying principles. Future work will therefore focus on improving the frame rate and on exploring new generative backbones to further push performance for high-quality ultra-low-bitrate semantic communication.

## REFERENCES

- [1] E. C. Strinati and S. Barbarossa, “6g networks: Beyond shannon towards semantic and goal-oriented communications,” *Computer Networks*, vol. 190, p. 107930, 2021.
- [2] D. Wheeler and B. Natarajan, “Engineering semantic communication: A survey,” *IEEE Access*, vol. 11, pp. 13 965–13 995, 2023.
- [3] H. Xie, Z. Qin, G. Y. Li, and B.-H. Juang, “Deep learning enabled semantic communication systems,” *IEEE Transactions on Signal Processing*, vol. 69, pp. 2663–2675, 2021.
- [4] Z. Weng, Z. Qin, and G. Y. Li, “Semantic communications for speech signals,” in *ICC 2021-IEEE International Conference on Communications*. IEEE, 2021, pp. 1–6.
- [5] H. Tong, Z. Yang, S. Wang, Y. Hu, W. Saad, and C. Yin, “Federated learning based audio semantic communication over wireless networks,” in *2021 IEEE Global Communications Conference (GLOBECOM)*. IEEE, 2021, pp. 1–6.
- [6] E. Grassucci, C. Marinoni, A. Rodriguez, and D. Comminiello, “Diffusion models for audio semantic communication,” in *ICASSP*. IEEE, 2024, pp. 13 136–13 140.
- [7] L. Qi, Z. Jia, J. Li, B. Li, H. Li, and Y. Lu, “Generative latent coding for ultra-low bitrate image and video compression,” *IEEE TCSVT*, 2025.
- [8] Z. Guo, Z. Jia, J. Li, X. Zhang, B. Li, and Y. Lu, “Generative latent video compression,” *arXiv preprint arXiv:2510.09987*, 2025.
- [9] Z. Jia, J. Li, B. Li, H. Li, and Y. Lu, “Generative latent coding for ultra-low bitrate image compression,” in *CVPR*, 2024, pp. 26 088–26 098.
- [10] F. Mentzer, G. D. Toderici, M. Tschannen, and E. Agustsson, “High-fidelity generative image compression,” *NeurIPS*, vol. 33, pp. 11 913–11 924, 2020.
- [11] E. Agustsson, M. Tschannen, F. Mentzer, R. Timofte, and L. V. Gool, “Generative adversarial networks for extreme learned image compression,” in *ICCV*, 2019, pp. 221–231.
- [12] E. Grassucci, S. Barbarossa, and D. Comminiello, “Generative semantic communication: Diffusion models beyond bit recovery,” *arXiv preprint arXiv:2306.04321*, 2023.
- [13] E. Grassucci, Y. Mitsufuji, P. Zhang, and D. Comminiello, “Enhancing semantic communication with deep generative models: An overview,” in *ICASSP*. IEEE, 2024, pp. 13 021–13 025.
- [14] E. Grassucci, J. Park, S. Barbarossa, S.-L. Kim, J. Choi, and D. Comminiello, “Generative ai meets semantic communication: Evolution and revolution of communication tasks,” *arXiv preprint arXiv:2401.06803*, 2024.
- [15] L. Guo, W. Chen, Y. Sun, B. Ai, N. Pappas, and T. Quek, “Diffusion-driven semantic communication for generative models with bandwidth constraints,” *IEEE Transactions on Wireless Communications*, 2025.
- [16] B. Li, Y. Liu, X. Niu, B. Bait, W. Han, L. Deng, and D. Gunduz, “Extreme video compression with prediction using pre-trained diffusion models,” in *2024 16th International Conference on Wireless Communications and Signal Processing (WCSP)*. IEEE, 2024, pp. 1449–1455.
- [17] Z. Li, Y. Zhou, H. Wei, C. Ge, and J. Jiang, “Towards extreme image compression with latent feature guidance and diffusion prior,” *IEEE TCSVT*, 2024.

- [18] S. Iwai, T. Miyazaki, and S. Omachi, "Semantically-guided image compression for enhanced perceptual quality at extremely low bitrates," *IEEE Access*, 2024.
- [19] R. Yang, R. Timofte, and L. Van Gool, "Perceptual learned video compression with recurrent conditional gan," in *IJCAI*, 2022, pp. 1537–1544.
- [20] Z. Yan, J. Pei, H. Wu, H. Tabassum, and P. Wang, "Semantic-aware adaptive video streaming using latent diffusion models for wireless networks," *arXiv preprint arXiv:2502.05695*, 2025.
- [21] W. Ma and Z. Chen, "Diffvc-osd: One-step diffusion-based perceptual neural video compression framework," *arXiv preprint arXiv:2508.07682*, 2025.
- [22] C. Li, G. Lu, D. Feng, H. Wu, Z. Zhang, X. Liu, G. Zhai, W. Lin, and W. Zhang, "Misc: Ultra-low bitrate image semantic compression driven by large multimodal model," *IEEE TIP*, 2024.
- [23] E. Lei, Y. B. Uslu, H. Hassani, and S. S. Bidokhti, "Text+ sketch: Image compression at ultra low rates," 2023.
- [24] P. Jiang, C.-K. Wen, S. Jin, and G. Y. Li, "Wireless semantic communications for video conferencing," *IEEE Journal on Selected Areas in Communications*, vol. 41, no. 1, pp. 230–244, 2022.
- [25] M. Yang, D. Gao, F. Xie, J. Li, X. Song, and G. Shi, "Sg2sc: A generative semantic communication framework for scene understanding-oriented image transmission," in *ICASSP*. IEEE, 2024, pp. 13486–13490.
- [26] D. Huang, F. Gao, X. Tao, Q. Du, and J. Lu, "Toward semantic communications: Deep learning-based image semantic coding," *IEEE Journal on Selected Areas in Communications*, vol. 41, no. 1, pp. 55–71, 2022.
- [27] J. Huang, C. Liu, and D. Liu, "Semantic segmentation-based low-rate image communication with diffusion models," in *2024 16th International Conference on Wireless Communications and Signal Processing (WCSP)*. IEEE, 2024, pp. 1412–1417.
- [28] C. Eteke, A. Griessel, W. Kellerer, and E. Steinbach, "Lossy coding for spatially adaptive conditioning in semantic image communication," in *VCIP*. IEEE, 2024, pp. 1–5.
- [29] Y. Gao, X. Pan, X. Li, and Z. Chen, "Why compress what you can generate? when gpt-4o generation ushers in image compression fields," in *ICCV*, 2025, pp. 371–381.
- [30] J. Park and S. W. Yoon, "Transmit what you need: task-adaptive semantic communications for visual information," *IEEE Journal on Selected Areas in Communications*, 2025.
- [31] C. Eteke, A. Griessel, W. Kellerer, and E. Steinbach, "Real-time semantic video communication with temporally consistent and controllable diffusion models," in *ICIP*. IEEE, 2025, pp. 361–366.
- [32] —, "High-fidelity semantic video communication with controllable image-to-video diffusion models," in *2025 IEEE International Symposium on Multimedia (ISM)*. IEEE, 2025.
- [33] Z. Qin, L. Liang, Z. Wang, S. Jin, X. Tao, W. Tong, and G. Y. Li, "Ai empowered wireless communications: From bits to semantics," *Proceedings of the IEEE*, 2024.
- [34] Y. Blau and T. Michaeli, "The perception-distortion tradeoff," in *CVPR*, 2018, pp. 6228–6237.
- [35] G. Konuko, G. Valenzise, and S. Lathuilière, "Ultra-low bitrate video conferencing using deep image animation," in *ICASSP*. IEEE, 2021, pp. 4210–4214.
- [36] J. Ballé, V. Laparra, and E. P. Simoncelli, "End-to-end optimized image compression," *ICLR*, 2017.
- [37] P. Dharwal and A. Nichol, "Diffusion models beat gans on image synthesis," *NeurIPS*, vol. 34, pp. 8780–8794, 2021.
- [38] R. Rombach, A. Blattmann, D. Lorenz, P. Esser, and B. Ommer, "High-resolution image synthesis with latent diffusion models," in *CVPR*, 2022, pp. 10684–10695.
- [39] L. Zhang, A. Rao, and M. Agrawala, "Adding conditional control to text-to-image diffusion models," in *ICCV*, 2023, pp. 3836–3847.
- [40] F. Pezzone, O. Musa, G. Caire, and S. Barbarossa, "Semantic-preserving image coding based on conditional diffusion models," in *ICASSP*. IEEE, 2024, pp. 13501–13505.
- [41] G. J. Sullivan, J.-R. Ohm, W.-J. Han, and T. Wiegand, "Overview of the high efficiency video coding (hevc) standard," *IEEE TCSVT*, vol. 22, no. 12, pp. 1649–1668, 2012.
- [42] B. Bross, Y.-K. Wang, Y. Ye, S. Liu, J. Chen, G. J. Sullivan, and J.-R. Ohm, "Overview of the versatile video coding (vvc) standard and its applications," *IEEE TCSVT*, vol. 31, no. 10, pp. 3736–3764, 2021.
- [43] Z. Jia, B. Li, J. Li, W. Xie, L. Qi, H. Li, and Y. Lu, "Towards practical real-time neural video compression," in *CVPR*, 2025.
- [44] R. Wan, Q. Zheng, and Y. Fan, "M3-cvc: Controllable video compression with multimodal generative models," in *ICASSP*. IEEE, 2025, pp. 1–5.
- [45] Q. Zhou, R. Li, J. Guo, Y. Huang, Z. Xu, L. Cui, and S. Guo, "Denc: Unleash neural codecs in video streaming with diffusion enhancement," in *Proceedings of the AAAI Conference on Artificial Intelligence*, vol. 39, no. 1, 2025, pp. 1192–1200.
- [46] A. Vaswani, N. Shazeer, N. Parmar, J. Uszkoreit, L. Jones, A. N. Gomez, Ł. Kaiser, and I. Polosukhin, "Attention is all you need," *NeurIPS*, vol. 30, 2017.
- [47] S. Luo, Y. Tan, L. Huang, J. Li, and H. Zhao, "Latent consistency models: Synthesizing high-resolution images with few-step inference," *arXiv preprint arXiv:2310.04378*, 2023.
- [48] T. Yin, M. Gharbi, R. Zhang, E. Shechtman, F. Durand, W. T. Freeman, and T. Park, "One-step diffusion with distribution matching distillation," in *CVPR*, 2024, pp. 6613–6623.
- [49] C. Eteke, A. Griessel, W. Kellerer, and E. Steinbach, "Bir-adapter: A parameter-efficient diffusion adapter for blind image restoration," *arXiv preprint arXiv:2509.06904*, 2025.
- [50] A. Kodaira, C. Xu, T. Hazama, T. Yoshimoto, K. Ohno, S. Mitsuhashi, S. Sugano, H. Cho, Z. Liu, M. Tomizuka *et al.*, "Streamdiffusion: A pipeline-level solution for real-time interactive generation," in *ICCV*, 2025, pp. 12371–12380.
- [51] M. Cordts, M. Omran, S. Ramos, T. Rehfeld, M. Enzweiler, R. Benenson, U. Franke, S. Roth, and B. Schiele, "The cityscapes dataset for semantic urban scene understanding," in *CVPR*, 2016.
- [52] M. Denninger, D. Winkelbauer, M. Sundermeyer, W. Boerdijk, M. Knauer, K. H. Strobl, M. Humt, and R. Triebel, "Blenderproc2: A procedural pipeline for photorealistic rendering," *Journal of Open Source Software*, vol. 8, no. 82, p. 4901, 2023. [Online]. Available: <https://doi.org/10.21105/joss.04901>
- [53] B. Calli, A. Walsman, A. Singh, S. Srinivasa, P. Abbeel, and A. M. Dollar, "Benchmarking in manipulation research: The YCB object and model set and benchmarking protocols," *IEEE Robotics and Automation Magazine*, pp. 36–52, Sep. 2015.
- [54] I. Loshchilov and F. Hutter, "Decoupled weight decay regularization," *ICLR*, 2019.
- [55] D. Podell, Z. English, K. Lacey, A. Blattmann, T. Dockhorn, J. Müller, J. Penna, and R. Rombach, "Sdxl: Improving latent diffusion models for high-resolution image synthesis," *ICLR*, 2024.
- [56] R. Timofte, E. Agustsson, S. Gu, J. Wu, A. Ignatov, and L. Van Gool, "Div2k dataset: Diverse 2k resolution high quality images as used for the challenges@ ntire (cvpr 2017 and cvpr 2018) and@ pirm (eccv 2018)," 2018.
- [57] S. Gu, A. Lugmayr, M. Danelljan, M. Fritzsche, J. Lamour, and R. Timofte, "Div8k: Diverse 8k resolution image dataset," in *ICCVW*. IEEE, 2019, pp. 3512–3516.
- [58] B. Lim, S. Son, H. Kim, S. Nah, and K. Mu Lee, "Enhanced deep residual networks for single image super-resolution," in *CVPR*, 2017, pp. 136–144.
- [59] X. Wang, L. Xie, C. Dong, and Y. Shan, "Real-esrgan: Training real-world blind super-resolution with pure synthetic data," in *ICCV*, 2021, pp. 1905–1914.
- [60] Y. Guo, C. Yang, A. Rao, Z. Liang, Y. Wang, Y. Qiao, M. Agrawala, D. Lin, and B. Dai, "Animatediff: Animate your personalized text-to-image diffusion models without specific tuning," *ICLR*, 2024.
- [61] T. Yin, Q. Zhang, R. Zhang, W. T. Freeman, F. Durand, E. Shechtman, and X. Huang, "From slow bidirectional to fast autoregressive video diffusion models," in *CVPR*, 2025, pp. 22963–22974.
- [62] K. Nan, R. Xie, P. Zhou, T. Fan, Z. Yang, Z. Chen, X. Li, J. Yang, and Y. Tai, "Openvid-1m: A large-scale high-quality dataset for text-to-video generation," *ICLR*, 2025.
- [63] R. Zhang, P. Isola, A. A. Efros, E. Shechtman, and O. Wang, "The unreasonable effectiveness of deep features as a perceptual metric," in *CVPR*, 2018, pp. 586–595.
- [64] Z. Huang, Y. He, J. Yu, F. Zhang, C. Si, Y. Jiang, Y. Zhang, T. Wu, Q. Jin, N. Champaisit, Y. Wang, X. Chen, L. Wang, D. Lin, Y. Qiao, and Z. Liu, "VBench: Comprehensive benchmark suite for video generative models," in *CVPR*, 2024.
- [65] G. J. Sullivan, J.-R. Ohm, W.-J. Han, and T. Wiegand, "Overview of the high efficiency video coding (hevc) standard," *IEEE TCSVT*, vol. 22, no. 12, pp. 1649–1668, 2012.
- [66] B. Bross, Y.-K. Wang, Y. Ye, S. Liu, J. Chen, G. J. Sullivan, and J.-R. Ohm, "Overview of the versatile video coding (vvc) standard and its applications," *IEEE TCSVT*, vol. 31, no. 10, pp. 3736–3764, 2021.